Ultra low water adhesive metal surface for enhanced corrosion protection†

Gang Wang,[a] Zhixiang Zeng,[b] Junjun Chen,[b] Mengya Xu,[b] Jingfang Zhu,[b] Shuan Liu,[b] Tianhui Ren*[a] and Qunji Xue[b]

A superhydrophobic surface with ultra low water adhesive force is fabricated on various metals for enhanced corrosion protection. The superhydrophobic surface is constructed by passivated zinc oxide (ZnO) and low surface energy poly(dimethylsiloxane) (PDMS). The process of wettability transformation and corrosion are evaluated by a salt spray test and electrochemical measurement. The superhydrophobic surface is separated layer-by-layer to reveal the function of each layer in corrosion protection. The surface adhesive force is applied as a novel metric for precisely determining the wettability state on the substrate surface. The results reveal that the ultra low water adhesive force of the superhydrophobic surface can effectively suppress water condensation on the metal surface which can suppress the transformation from the Cassie to Wenzel state. The superhydrophobic surface can effectively inhibit corrosion because of the synergistic effect of the triple layered protection system of air, PDMS and ZnO.

Introduction

There is a great demand for metals in daily life, in the construction, military and industry because of their excellent conductivity, thermal conductivity, great strength and machinability. However, the thermodynamic instability of metal atoms are easy to translate into its compounds under hydrothermal and corrosive conditions which results in a corrosion reaction. The degradation or failure of the metal materials caused by the corrosion reactions not only brings huge economic loss but also threatens the safety of human life. So, where there is a metal, there is a need for corrosion protection. Thus, effective protection technology is necessary to inhibit the corrosion reaction. Up to now, lots of methods are used to protect metals against corrosion such as cathodic protection, protective coatings, corrosion inhibitors and alloying element addition.[1–6] In these methods, coating is one of the most effective and economical ways to inhibit the metal corrosion which can obstruct the contact of the corrosive medium with the metal. Generally, there are three methods applied to improve the protective performance of the coatings. Firstly, corrosion inhibitors are added into the coating to inhibit the metal corrosion reaction underneath the coating.[7–9] Secondly, fillers or pigments, such as graphene, nanoclay, zinc oxide (ZnO) and silicon dioxide, are added into the coating to elongate the diffusion path of the corrosive media through the coating.[10–14] Thirdly, high density, highly crosslinked, thicker and self-healing coatings are needed to reduce the coating permeability.[15–17] However, the drawbacks of poor dispersion, toxicity, negative effect to mechanical property and long response time limit their wide application.

Compared with the previously mentioned methods, a superhydrophobic surface with a liquid contact angle higher than 150° and the sliding angle lower than 10° can effectively prevent the contact between the corrosive liquid and the metal surface which inhibits corrosion.[18] In addition, the low water adhesion of the superhydrophobic surface is widely used for self-cleaning, antifogging, and drag reduction, and so on.[19,20] Thus, the superhydrophobic surface is a promising coating to prevent corrosion because of its excellent water resistance.

In recent years, lots of superhydrophobic surfaces were prepared by bottom-up (layer-by-layer assembly, dip-coating, spin-coating, spray-coating, chemical vapor deposition and phase-separation) and top-down (etching and lithography) approaches.[21] Boinovich *et al.* fabricated a superhydrophobic oxidized surface of aluminum alloys with enhanced resistance to pitting corrosion in sodium chloride (NaCl) solutions using a nanosecond laser treatment.[22] Xiao *et al.* prepared superhydrophobic copper oxide nanoneedle array films for the enhancement of corrosion resistance of copper substrates by

[a]*Key Laboratory for Thin Film and Microfabrication, School of Chemistry and Chemical Engineering, Shanghai Jiao Tong University, Shanghai 200240, P. R. China. E-mail: thren@sjtu.edu.cn*

[b]*Key Laboratory of Marine Materials and Related Technologies, Zhejiang Key Laboratory of Marine Materials and Protective Technologies, Ningbo Institute of Materials Technology and Engineering, Chinese Academy of Sciences, Ningbo, 315201, P. R. China*

electrochemical anodization.[23] However, creating a superhydrophobic surface on a metal surface is still a challenging task.[24] Furthermore, the diverse steps, high technique requirements and specificity of substrate for creating superhydrophobic coatings were the main constraints to the wide application of superhydrophobic coatings. Some superhydrophobic anticorrosion coatings are only suitable for a specific metal. A common approach to fabricating a superhydrophobic anticorrosion coating on metal is needed.

According to previous papers in the literature, a stable air barrier trapped in hierarchical roughness and low contact area between the corrosion liquid and the solid surface are the fundamental mechanisms of superhydrophobic surfaces for corrosion resistance.[25] Therefore, a Cassie state is essential for superhydrophobic surfaces to inhibit corrosion. It is reported that the superhydrophobic surface lost corrosion resistance during long-term contact of corrosion solution because of the transformation from a Cassie to a Wenzel state.[22,26,27] So more dense, passivated and "Cassie-stable" superhydrophobic surfaces are needed to enhance the anticorrosion property.

In this research, a superhydrophobic surface constructed with passivated ZnO and low surface energy poly(dimethylsiloxane) (PDMS) was fabricated on various metals to give corrosion resistance. The process of wettability transformation and corrosion is simulated by the salt spray test, which can be clearly observed. The superhydrophobic surface is separated layer-by-layer for corrosion testing to reveal the function of each layer in corrosion resistance. The surface adhesive force is applied as a novel metric for precisely determining the wettability state on the substrate surface. Electrochemical measurements are used to evaluate the anticorrosion property of the sample. The results demonstrate that the triple layered protection system of the as-prepared superhydrophobic surface presents outstanding corrosion resistance in metal protection.

Results and discussion

Previous studies demonstrate that the best water contact angle (WCA) of smooth surfaces do not exceed 125–130°.[28] Surface roughness is a key factor in creating a superhydrophobic surface which can amplify the intrinsic wetting property according to the Cassie–Baxter model. Thus, a superhydrophobic surface can be attained using low energy materials with an hierarchical rough surface. ZnO is an oxide semiconductor with special optical, electrical, chemical, biological and non-toxic properties and has been used as pigment in coatings to improve metal corrosion protection.[13] Furthermore, the ZnO with diverse and versatile morphologies from one-dimensional to three-dimensional nanostructures can be synthesized at low temperature on a wide range of substrates without using sophisticated or expensive equipment.[29] PDMS is one of the most important high performance polymers and widely used in corrosion resistance because of its hydrophobicity, thermal stability, adhesivity, flexibility and chemical inertness. Furthermore, the crosslinked PDMS will form a barrier layer which can effectively inhibit corrosion liquid infiltration. Therefore, a superhydrophobic coating was fabricated with anticorrosion properties by two simple steps of aligned ZnO nanorod array construction and low energy crosslinked PDMS modification. The fabrication procedure is shown in Scheme 1.

The aligned ZnO nanorod array film is constructed on the low alloy steel substrate *via* a simple hydrothermal method. Compared with the smooth uncoated steel substrate (Fig. S1a†), there is a uniform, dense and white film on the steel substrate (Fig. 1a). It is seen from the magnified scanning electron microscopy (SEM) image (Fig. 1b) that the film is composed of aligned ZnO nanorod arrays. The length of a single ZnO nanorod is about 4.7 μm which is arranged vertically on the substrate surface (Fig. 1c). Every ZnO nanorod is assembled by hexagonal nanosheets fabricated step-by-step in layers and it presents as a cone shaped rod. These nanosheets are about 20–50 nm in thickness on average (Fig. 1d). Between the nanosheets, there are nanogrooves. The hierarchical structure which combines micro- and nano-structures and tightly packed rods are beneficial for air capture which is significant for superhydrophobic surface construction. In order to get superhydrophobicity, low energy PDMS is coated on the aligned ZnO nanorod arrays by dip coating. In Fig. 1e, a thin film can be seen on the aligned ZnO nanorod arrays which is marked by red arrows. In the transmission electron microscopy (TEM) images (Fig. S2†), it can be seen that the crystal surface of ZnO (dark area) is covered by a crosslinked PDMS film (light color area) with the thickness of 65.86–6.13 nm.

The structure and phase composition of the as-prepared ZnO coating is revealed in its X-ray diffraction (XRD) pattern. As shown in Fig. 2a, there are sharp peaks of iron (Fe) marked with diamonds in the XRD pattern of the uncoated substrate. Compared with a ZnO coated substrate, typical diffraction peaks of ZnO are detected. The ZnO diffraction peaks marked with spades match well with standard hexagonal ZnO crystallography (JCPDS card no. 36-1451). The previous results indicate that the hierarchical aligned ZnO nanorod arrays are successfully coated on the substrate. The surface composition of the ZnO and ZnO/PDMS coated substrate was analyzed using X-ray photoelectron spectroscopy (XPS). In the XPS survey

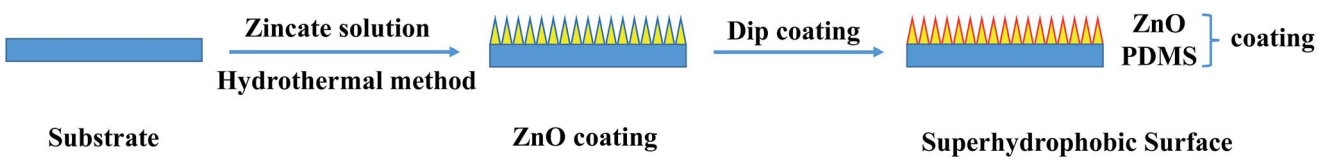

Scheme 1 Schematic illustration of the fabrication process for the ultra low water adhesive metal surface.

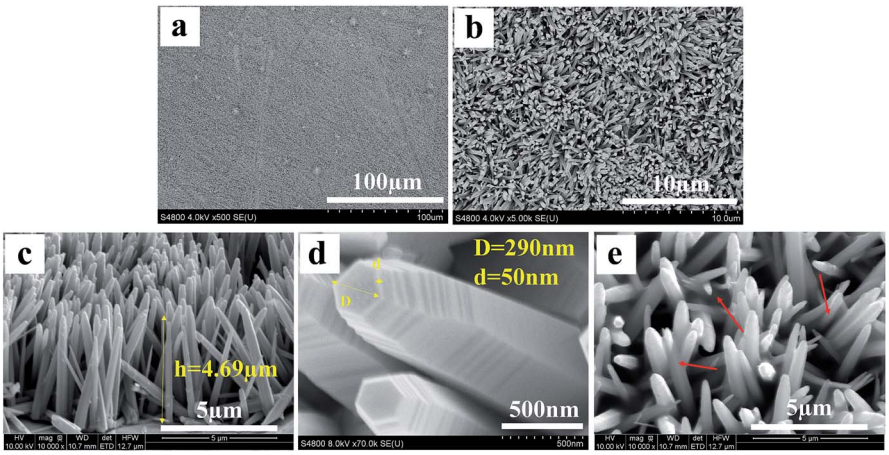

Fig. 1 Scanning electron microscopy (SEM) images of ZnO and ZnO/PDMS coated substrates. (a) Large-area view of ZnO coated substrate surface. (b) The higher magnification SEM images of the ZnO coated substrate surface. (c) SEM side view of the aligned ZnO nanorod array-coated substrate surface. (d) SEM image of a single ZnO nanorod. (e) The SEM image of ZnO/PDMS coated substrate surface.

spectrum (Fig. 2b), the elements of the ZnO coated substrate are carbon, oxygen and zinc (Zn) without silicon. After PDMS coating, all peaks corresponding to the ZnO coated substrate and the peak of silicon appears at 103 eV and these agree well with results reported in the literature. The content of every element is shown in Table S1.† The content of elemental silicon is up to 22.46%. The chemical composition and distribution of the ZnO/PDMS coated substrate was characterized using Fourier transform infrared spectroscopy (FTIR), energy dispersive X-ray spectrometry (EDS) and chemical element mapping images (Fig. S3†). Therefore, the coatings of ZnO and PDMS were successfully prepared on the substrate.

The water wettabilities of the samples are shown in Fig. 3. The changes of WCA of the four samples were recorded using a contact angle meter (Fig. 3a). The substrate is hydrophobic with a WCA of 109°. Even after the low surface energy material of PDMS was modified, the WCA was 114° which is still much lower than 150°. Although the surfaces of substrate and substrate/PDMS are hydrophobic, the hydrophobicity of the two surfaces seemed unstable. As time goes on, the WCA of the substrate and substrate/PDMS samples declined by 20° in 160 s. The surface of the substrate/ZnO sample is hydrophilic. The WCA of its surface declines significantly from 120° to 9° in

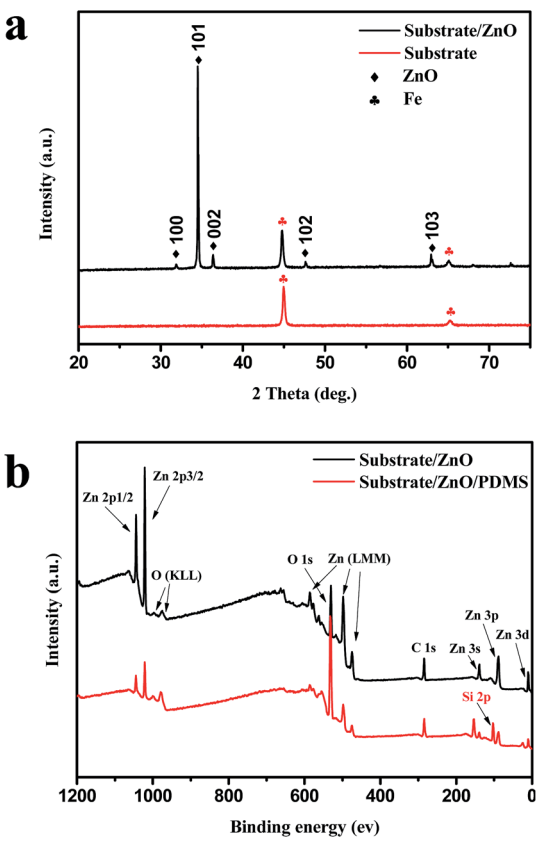

Fig. 2 Chemical composition analysis of various surfaces. (a) XRD patterns, (b) XPS survey spectrum of ZnO and ZnO/PDMS films.

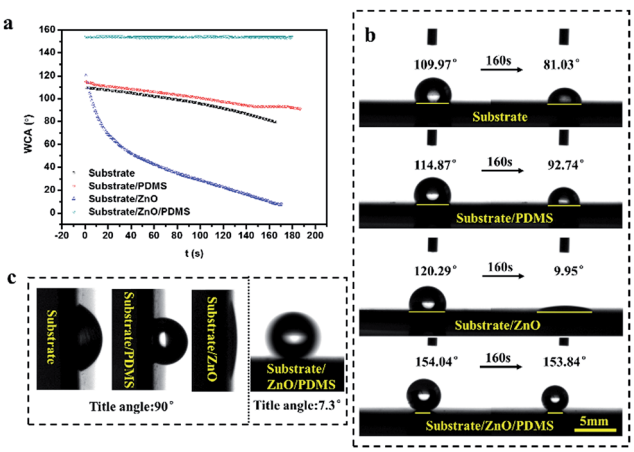

Fig. 3 The water wettability of the four samples. (a) The dynamic WCAs of the four samples. (b) The changes of contact diameter of water droplets of the four samples. (c) The water sliding angles of the four samples.

160 s. Combined with the hierarchical structure of ZnO and the low surface energy material of crosslinked PDMS, the surface of the substrate/ZnO/PDMS is superhydrophobic with a stable WCA of 154°. Teisala *et al.* studied the contact angle and contact diameter of evaporating water droplets which revealed the liquid adhesion behaviour on the different surfaces.[30] To investigate the wettability of various surfaces, the shape changes of water droplets were recorded on different surfaces (Fig. 3b). In Fig. 3b, there are no changes of the contact diameter of water droplets on the two hydrophobic surface of substrate and substrate/PDMS. The decline of water contact angle in Fig. 3a is because of to the volatilization of water droplet. To the hydrophilic substrate/ZnO surface, the water contact diameter is extended. Water droplet fast spreads out the substrate/ZnO surface and they were found to lose their spherical shape. The water contact diameter of the substrate/ZnO/PDMS surface is the shortest and remains stable throughout the evaporation process. In Fig. 3c, it can be seen that the substrate, ZnO coated and PDMS coated substrates have a high adhesive surface. The water droplets on these surfaces do not fall even if the surfaces are tilted 90°, which indicates the droplet is in the Wenzel state. Unlike these high adhesive surfaces, the droplet can easily roll from the substrate/ZnO/PDMS surface with a sliding angle of 7.3°. Thus, the advancing (adv) and receding (rec) contact angles can effectively reflect the wettability of liquid. The adv and rec contact angles for the surfaces were measured using the increment–decrement method (Table 1). The results of adv and rec contact angles reveal that the water droplets are in the Wenzel state on the substrate, substrate/ZnO and substrate/PDMS and in the Cassie state on substrate/ZnO/PDMS.

In order to reflect the interaction between water and sample surface more accurately, the adhesive behaviors of the samples were recorded using a microbalance detector and a high speed camera. Fig. 4 and 5 reveal typical force curves of water adhesion and adhesive behaviors of different samples, respectively. In Fig. 5a and b, which are the hydrophobic surfaces of uncoated substrate and PDMS coated substrate, it can be seen that the high surface adhesion force makes the water droplet break and remain on the substrate in the process of detachment. The surface of the ZnO coated substrate is hydrophilic. When the sample contacts with a water droplet, water is attracted to the sample surface with a large part of the water remaining on it after detachment (Fig. 5c). The maximum force (F_c) of these three samples represent the breaking force between the water and cannot represent the adhesive force between the water and the sample surface. Combined with the results of contact angle measurement, it can be concluded that water on these surfaces is in the Wenzel state. To the superhydrophobic surface, the adhesive force curve is distinct from that of the previous three samples (Fig. 4d). The water droplet remains intact in the whole process. F_c (6.2×10^{-6} N) represents the adhesive force between the water and the sample surface. Such a low value of adhesive force indicates that the water droplet with a weight higher than 6.2×10^{-4} g can detach from the as-prepared superhydrophobic surface under gravity. Calculated using the equation presented by Cassie and Baxter: $\cos\theta_r = f_1 \cos\theta - f_2$, where θ_r is the contact angle on a rough surface, θ is the intrinsic contact angle on a corresponding smooth surface (110° of PDMS), f_1 and f_2 are the area fractions of the liquid droplet when it makes contact with the solid surface and air, respectively, and $f_1 + f_2 = 1$, 85% of the rough surface area is covered by the air, and only 15% is in contact directly with water.[31] So, there is a stable air layer trapped in the hierarchical structure which minimizes the contact area between the water droplet and the superhydrophobic surface. The water droplet on the substrate/ZnO/PDMS surface is supported by the trapped air (Cassie state), which interprets the low sliding angle and adhesive force. Therefore, the air barrier and low water contact area will effectively inhibit the corrosion liquid permeation.

Table 1 Water contact angles and hysteresis of various surfaces

Surface	Static angle	Adv angle	Rec angle	Hysteresis
Substrate	109.97°	110.53°	84.19°	26.34°
Substrate/PDMS	114.87°	115.27°	92.12°	23.15°
Substrate/ZnO	0°	—	—	—
Substrate/ZnO/PDMS	154.04°	154.51°	147.27°	7.24°

Electrochemical measurement was used to evaluate the corrosion behavior of each layer of the superhydrophobic coatings in a 3.5 wt% NaCl aqueous solution. All samples were immersed for 2 h to ensure the steady state was reached. Fig. 6a depicts the polarization curves of uncoated, PDMS, ZnO and ZnO/PDMS coated substrate in 3.5 wt% NaCl solution, and the corrosion parameters, namely corrosion current density (i_{corr}) and corrosion potentials (E_{corr}) calculated from the Tafel zone are shown in Table 2. A lower i_{corr} and more positive E_{corr} usually indicate a better corrosion resistance of the coating/metal system. The i_{corr} of PDMS (4.26×10^{-7} A cm^{-2}) and ZnO coated substrate (1.86×10^{-7} A cm^{-2}) are similar to that of the uncoated substrate (3.82×10^{-7} A cm^{-2}), suggesting that substrate coated with single PDMS or ZnO has little protective performance. However, the i_{corr} of the ZnO/PDMS coated substrate (3.15×10^{-9} A cm^{-2}) decreased by more than two orders of magnitude as compared to that of the other three samples, indicating its excellent anticorrosion performance. The E_{corr} of the superhydrophobic surface (−0.339 V) is more positive than that of the other three samples. Electrochemical impedance spectroscopy (EIS) is an effective and non-destructive method to investigate anticorrosion behavior of coatings. Fig. 6b and d are the Nyquist and Bode plots of uncoated, PDMS, ZnO and ZnO/PDMS coated substrate in 3.5 wt% of NaCl solution (Fig. 6c is the magnified Nyquist plots of Fig. 6b in the high frequency region). These four coating/substrate systems have one capacitive arc during the whole test frequency (from 10^5 to 10^{-2} Hz). The capacitive arc diameter of the ZnO/PDMS coated substrate is much bigger than that of the other three samples. Usually, the impedance modulus at low frequency (such as $|Z|_{0.01\ Hz}$) represents the ability of the coating to impede corrosive media, which is inversely proportional to the corrosion rate.[32,33] The $|Z|_{0.01\ Hz}$ value of the ZnO/PDMS coated substrate was 398.1 kΩ cm^2 after 2 h immersion, which was much higher than that of uncoated substrate

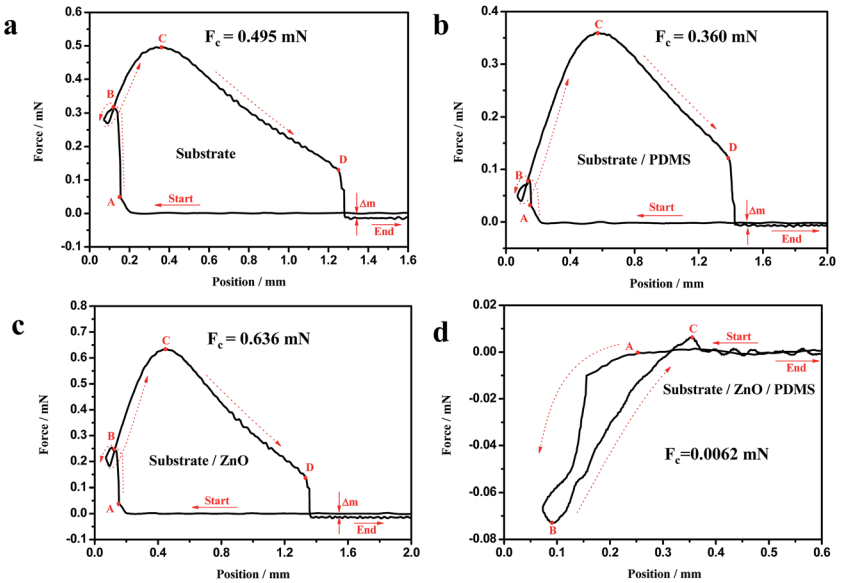

Fig. 4 Adhesive force as a function of motor position for the (a) uncoated substrate, (b) PDMS coated substrate, (c) ZnO coated substrate and (d) ZnO/PDMS coated substrate.

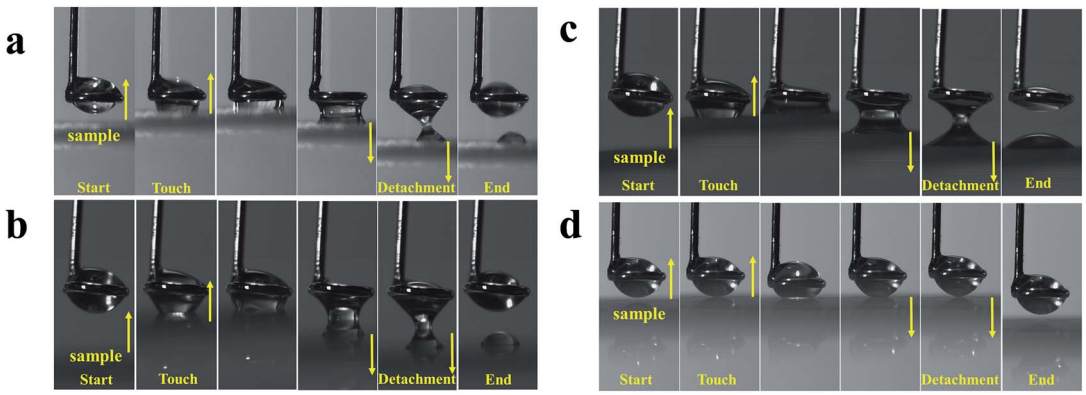

Fig. 5 High speed camera photographs of adhesive behavior for the (a) uncoated substrate, (b) PDMS coated substrate, (c) ZnO coated substrate and (d) ZnO/PDMS coated substrate.

(3.16 kΩ cm^2), ZnO coated substrate (3.31 kΩ cm^2) and PDMS coated substrate (3.24 kΩ cm^2). Both the polarization curves and EIS results clearly demonstrated that the ZnO/PDMS coated substrate exhibited the best anticorrosion performance. In addition, the E_{corr} of the ZnO coated substrate shifts in the positive direction, which indicates that the ZnO coating has some capability for anticorrosion. In 48 h of immersion in 3.5 wt% NaCl solution (Fig. 6e), the superhydrophobic ZnO/PDMS film exhibits a high $|Z|$ value of about 10^5 Ω cm^2 in the low frequency which reveals its long-term durability.

The previously described electrochemical experimental was implemented under a continuous corrosion liquid phase. The trapped air in the hierarchical structure of the superhydrophobic surface remains stable between the corrosion liquid and the solid surface. So, the stable Cassie state endows the superhydrophobic surface with an excellent anticorrosion property, as mentioned in research reported previously.[23,34] However, some studies state that the rough surface without superhydrophobicity or a superhydrophobic surface at Wenzel state have worse corrosion resistance than the bare substrate because it is easy for the corrosion liquid to penetrate of the substrate.[35,36] Vapor is undesirable to the superhydrophobic surface. The tiny condensed droplets [in the range of femtoliters (fL) to microliters (μL)] will get trapped in the texture in a sticky Wenzel state, which will destroy the superhydrophobicity of the materials.[37] Thus, the corrosion resistance of the as-prepared sample surfaces was further investigated in a salty fog. Fig. 7 shows the digital pictures of the samples after the 144 h salt spray test. The anticorrosion ability of the three coatings are obvious. As seen in Fig. 7, the hydrophobic uncoated and PDMS coated substrates rust uniformly and heavily only in 2 h. There are some corrosion spots on the surface of the hydrophilic ZnO coated substrate after 2 h, and the corrosion spots increase and grow slowly over time. To the superhydrophobic ZnO/PDMS

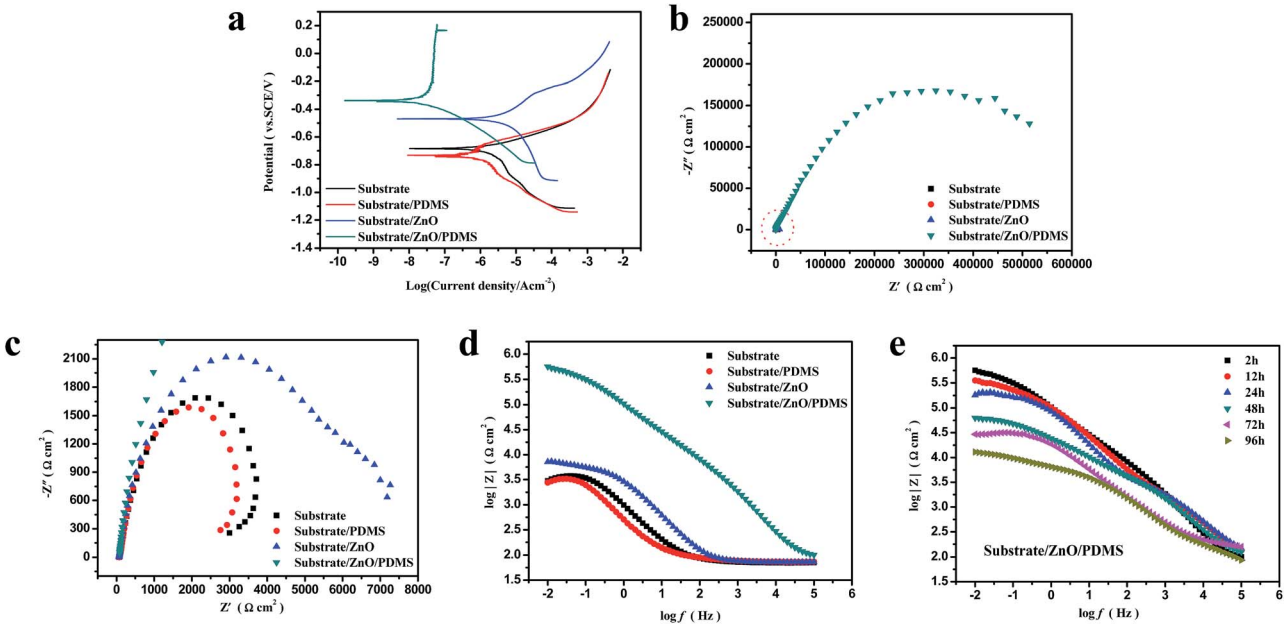

Fig. 6 (a) Potentiodynamic polarization curves, (b) Nyquist plots, (c) the magnified Nyquist plots of (b) in the high frequency region, and (d) Bode plots of uncoated substrate, PDMS coated substrate, ZnO coated substrate and ZnO/PDMS coated substrate after immersion in a 3.5 wt% NaCl aqueous solution for 2 h. (e) Bode |*Z*| *versus* frequency plots of the substrate/ZnO/PDMS samples immersed in 3.5 wt% NaCl solution for different times.

Table 2 E_{corr} and i_{corr} for uncoated substrate, PDMS coated substrate, ZnO coated substrate and ZnO/PDMS coated substrate after immersion in a 3.5 wt% NaCl aqueous solution for 2 h

Sample	Substrate	Substrate/PDMS	Substrate/ZnO	Substrate/ZnO/PDMS
i_{corr} (A cm^{-2})	3.82×10^{-7}	4.26×10^{-7}	1.86×10^{-7}	3.15×10^{-9}
E_{corr} (V)	−0.682	−0.739	−0.467	−0.340

coated substrate, no rust can be seen on it in 120 h, which indicates its excellent anticorrosion property in a salty fog condition. In the testing process, it can be seen that the salty fog forms a continuous water film on the uncoated, PDMS coated and ZnO coated substrate surfaces. Although the uncoated and PDMS coated substrate are hydrophobic, the corrosion products

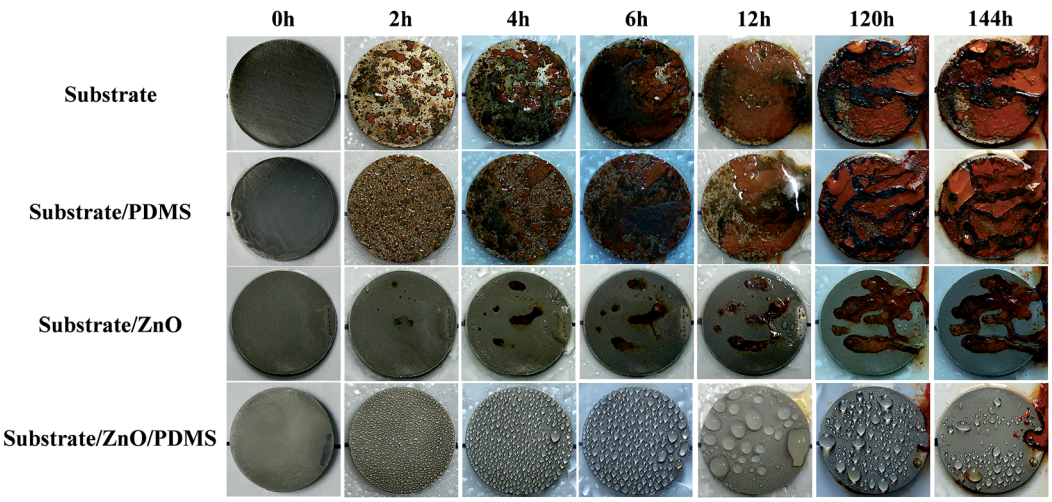

Fig. 7 Photographs of the salt spray tests of the substrate, substrate/PDMS, substrate/ZnO, and substrate/ZnO/PDMS samples at different exposure times.

change their surfaces from hydrophobicity to hydrophilicity. The salty fog first condenses on the superhydrophobic surface, forming tiny droplets stuck on the surface. As time goes by, the condensed saline water droplets grow larger. When the saline water droplets grow big enough, they fall off the surface and re-condense. Therefore, the saline water cannot gather on the superhydrophobic surface which can inhibit corrosion. During prolonged testing time, some large droplets are stuck on the surface in the Wenzel state and the corrosion appears after 144 h.

Using the water adhesive force curves, the anticorrosion behaviors of the four samples were determined. For the uncoated surface, it is hydrophobic but has a high adhesive surface. Corrosion easily occurs on its surface without coating protection. Because of the corrosion products, the uncoated surface changes from hydrophobic to hydrophilic which will accelerate corrosion. It is generally known that a dense and uniform coating is difficult to obtain, especially with a thin coating. For the PDMS coated substrate surface, the corrosion solution easily gathers on its surface and permeates into the pinholes and cracks (Fig. S1†) and it forms a Wenzel state because of the high adhesive force. Although the ZnO coated substrate is superhydrophilic, the anticorrosion property of the ZnO coated substrate is better than that of uncoated and PDMS coated substrates according to the results of electrochemical measurement and salt spray test. The anticorrosion property can only be ascribed to the passivation layer of ZnO. In Fig. S4,† there is some Fe element exposed in the chemical element mapping images of the ZnO coated substrate which causes the local corrosion. However, the superhydrophobic surface has the best anticorrosion property. So, it is considered that there are three stages in the anticorrosion process of the superhydrophobic surface (Fig. 8). Stage one, compared with the ordinary hydrophobic surface, the ultra low water adhesive force of the superhydrophobic surface can effectively expel the corrosion liquid. The corrosion liquid cannot gather on the superhydrophobic surface which suppresses the transformation from the Cassie state to the Wenzel state. Stage two, a stable air layer covers the superhydrophobic surface which can effectively inhibit corrosion liquid permeation and reduce the contact area. Stage three, the synergistic effect of the triple layered protection system of air, PDMS and ZnO which act as diffusion barrier can suspend the corrosion.

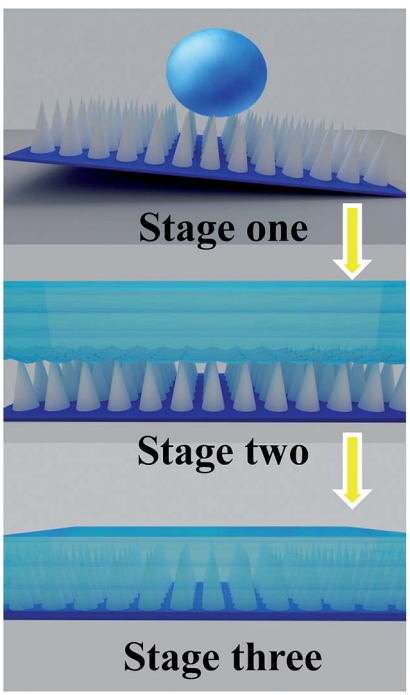

Fig. 8 A sketch of the three stages in the anticorrosion process of the superhydrophobic surface.

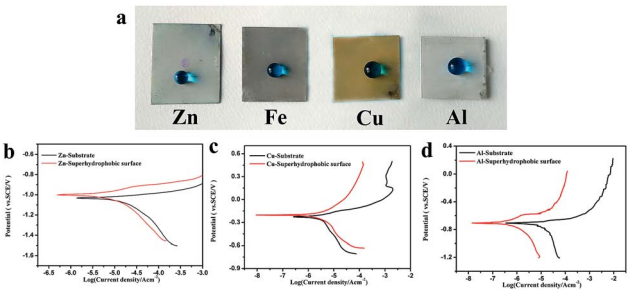

Fig. 9 (a) Digital photo of the water droplets on various superhydrophobic metal surfaces. Corrosion resistance of (b) uncoated Zn and superhydrophobic coated Zn, (c) uncoated copper (Cu) and superhydrophobic coated Cu and (d) uncoated aluminium (Al) and superhydrophobic coated Al.

In addition, the superhydrophobic coating can be fabricated on various metal surfaces, such as Zn, Fe, Cu and Al, which expands its scope of application (Fig. 9a). Based on the results of the electrochemical measurement (Fig. 9b–d and Table S2†), the as-prepared superhydrophobic coating can protect the metals from corrosion well.

Conclusions

In conclusion, superhydrophobic surfaces were fabricated by constructing them with ultra low water adhesive force using passivated ZnO and low surface energy PDMS on various metals for enhanced corrosion protection. The process of wettability transformation and corrosion was evaluated using a salt spray test and electrochemical measurements. The superhydrophobic surface was separated layer-by-layer for corrosion testing to reveal the function of each layer in the corrosion resistance. The surface adhesive force was applied as a novel metric for precisely determining the wettability state on the substrate surface. The results revealed that the ultra low water adhesive force of the superhydrophobic surface can effectively expel the corrosion liquid. The corrosion liquid cannot gather on the superhydrophobic surface which suppresses the transformation from the Cassie state to the Wenzel state. The stable air layer covers the superhydrophobic surface, which can effectively inhibit the corrosion liquid permeation and reduce the contact area. The synergistic effect of the triple layered

protection system of air, PDMS and ZnO, which acts as a diffusion barrier can interrupt the corrosion. In addition, the superhydrophobic surfaces can be fabricated on various metal surfaces and protect them well from corrosion.

Experimental

Materials

The low alloy steel (the elemental concentration of the low alloy steel is shown in Fig. S6†), Zn, Cu and Al foils were purchased from a local store. PDMS prepolymer and curing agent (Sylgard 184) were purchased from Dow Corning. All the chemical regents were purchased from Aladdin Reagents and used without further purification.

Coating fabrication

The metal foil was cleaned sequentially with acetone and deionized water and then dried at 80 °C. The aligned ZnO nanorod array coated substrate was prepared using a one-step hydrothermal route at a relatively lower temperature (95 °C). The metal foil with a radius of 1 cm was immersed vertically in a 100 mL aqueous solution, which consisted of 0.01 mol of zinc nitrate hexahydrate ($Zn(NO_3)_2 \cdot 6H_2O$), 0.002 mol of ammonium chloride, 0.01 mol of urea and 5 mL of 25% ammonia, and then the system was sealed and heated to 90 °C for 1 h. Subsequently, the as-prepared sample was washed with deionized water and dried at 80 °C.

The superhydrophobic sample was obtained using a dip-coating method. The as-prepared aligned ZnO nanorod array coated substrate was dipped into a PDMS solution, which consisted of 1 g of PDMS, 0.1 g of curing agent and 100 mL of ethyl acetate. Finally, the as-prepared sample was cured at 80 °C for 6 h to obtain superhydrophobicity.

Coating characterization

The surface microstructures were characterized using SEM (Quanta 250 FEG, FEI, USA) and TEM (Tecnai F20, FEI, USA), and the chemical composition and element mapping of the films were performed using energy dispersive X-ray spectroscopy (EDS). The XRD patterns of the uncoated and ZnO coated substrates were measured using XRD (D8 Advance, Bruker-AXS, Germany) with CuKα radiation, $\lambda = 1.542$ Å. Surface composition was examined using FTIR (Nicolet 6700, Thermo Fisher Scientific, US) and X-ray photoelectron spectroscopy (XPS) (Axis Ultra DLD, Kratos Analytical, UK). The water contact angles were measured using a contact angle meter (OCA 20, DataPhysics, Germany). A water droplet with a volume of 2.0 μL was dropped carefully onto the substrate surface. Water sliding angles were obtained by gradually inclining the tilting stage until the water droplet began to roll. At least five locations of the same surface were tested in order to get the average value. Electrochemical measurements were performed using an electrochemical workstation (ModuLab ECS, Solartron Analytical Ltd., UK) at room temperature with a traditional three electrode system. The 3.5 wt% NaCl aqueous solution, platinum stick electrode and saturated calomel electrode (SCE) were used as the electrolyte, counter electrode and reference electrode, respectively. The potential was measured between −400 and +800 mV *versus* SCE at a scan rate of 0.5 mV s^{-1}. All the samples were immersed for 2 h to ensure the steady state was reached. The corrosion resistance properties of the substrates were studied using a salt spray test (Q-FOG CCT-1100, Q-Lab, USA) (NaCl 3.5 wt% solution) (according to ASTM B117,[38] where the chamber temperature was controlled at 35 °C, the salt solution used was 3.5 wt% NaCl and its pH value was about 7.0). The surface adhesive forces of the substrates were measured using a dynamic contact angle measuring device and a tension meter (DCTA 21, DataPhysics). The details are shown in Fig. S5.† The adhesive behavior of droplet was recorded using a high speed camera at a rate of 1000 frames per second (FASTCAM Mini UX100, Photron Limited, Japan).

Acknowledgements

Project No. 51475450 and 51335010 were supported by the National Nature Science Foundation of China. This research is also based upon work funded by the China Postdoctoral Science Foundation (No. 2015M580528), the National Basic Research Program of China (No. 2014CB643302), the Zhejiang Provincial Innovation Team (Grant No. 2011R50006), the Ningbo social benefiting plan by science and technology (2015C50055), and the Ningbo Municipal Innovation Team (Grant No. 2011B81001). The authors are grateful to the National Natural Science Foundation of China (Grant No. 21272157) for the financial and technical support of the work reported in this paper.

Notes and references

1 W. X. Guo, X. Y. Li, M. X. Chen, L. Xu, L. Dong, X. Cao, W. Tang, J. Zhu, C. J. Lin, C. F. Pan and Z. L. Wang, *Adv. Funct. Mater.*, 2014, **24**, 6691–6699.
2 P. P. Deshpande, N. G. Jadhav, V. J. Gelling and D. Sazou, *J. Coat. Technol. Res.*, 2014, **11**, 473–494.
3 M. F. Montemor, *Surf. Coat. Technol.*, 2014, **258**, 17–37.
4 D. Kesavan, M. Gopiraman and N. Sulochana, *Chem. Sci. Rev. Lett.*, 2012, **1**, 1.
5 D. S. Gandel, M. A. Easton, M. A. Gibson, T. Abbott and N. Birbilis, *Corros. Sci.*, 2014, **81**, 27–35.
6 Y. Ding, C. Wen, P. Hodgson and Y. Li, *J. Mater. Chem. B*, 2014, **2**, 1912–1933.
7 J. Fu, T. Chen, M. Wang, N. Yang, S. Li, Y. Wang and X. Liu, *ACS Nano*, 2013, **7**, 11397–11408.
8 D. G. Shchukin, M. Zheludkevich, K. Yasakau, S. Lamaka, M. G. Ferreira and H. Moehwald, *Adv. Mater.*, 2006, **18**, 1672–1678.
9 M. J. Hollamby, D. Fix, I. Dönch, D. Borisova, H. Möhwald and D. Shchukin, *Adv. Mater.*, 2011, **23**, 1361–1365.
10 Y. H. Yu, Y. Y. Lin, C. H. Lin, C. C. Chan and Y. C. Huang, *Polym. Chem.*, 2014, **5**, 535–550.
11 D. Prasai, J. C. Tuberquia, R. R. Harl, G. K. Jennings and K. I. Bolotin, *ACS Nano*, 2012, **6**, 1102–1108.

12 E. Faure, E. Halusiak, F. Farina, N. Giamblanco, C. Motte, M. Poelman, C. Archambeau, C. V. D. Weerdt, J. Martial, C. Jérôme, A. S. Duwez and C. Detrembleur, *Langmuir*, 2012, **28**, 2971–2978.
13 L. Ejenstam, A. Swerin, J. Pan and P. M. Claesson, *Corros. Sci.*, 2015, **99**, 89–97.
14 S. H. Sonawane, B. M. Teo, A. Brotchie, F. Grieser and M. Ashokkumar, *Ind. Eng. Chem. Res.*, 2010, **49**, 2200–2205.
15 D. Wang and G. P. Bierwagen, *Prog. Org. Coat.*, 2009, **64**, 327–338.
16 G. Wu, J. An, D. Sun, X. Tang, Y. Xiang and J. Yang, *J. Mater. Chem. A*, 2014, **2**, 11614–11620.
17 D. V. Andreeva, D. Fix, H. Möhwald and D. G. Shchukin, *Adv. Mater.*, 2008, **20**, 2789–2794.
18 C. H. Xue and J. Z. Ma, *J. Mater. Chem. A*, 2013, **1**, 4146–4161.
19 K. Liu, M. Cao, A. Fujishima and L. Jiang, *Chem. Rev.*, 2014, **114**, 10044–10094.
20 K. Liu, Y. Tian and L. Jiang, *Prog. Mater. Sci.*, 2013, **58**, 503–564.
21 L. Yao and J. He, *Prog. Mater. Sci.*, 2014, **61**, 94–143.
22 L. B. Boinovich, A. M. Emelyanenko, A. D. Modestov, A. G. Domantovsky and K. A. Emelyanenko, *ACS Appl. Mater. Interfaces*, 2015, **7**, 19500–19508.
23 F. Xiao, S. Yuan, B. Liang, G. Li, S. O. Pehkonen and T. Zhang, *J. Mater. Chem. A*, 2015, **3**, 4374–4388.
24 K. Liu and L. Jiang, *Nanoscale*, 2011, **3**, 825–838.
25 R. Ramachandran and M. Nosonovsky, *Phys. Chem. Chem. Phys.*, 2015, **17**, 24988–24997.
26 L. Liu, R. Chen, W. Liu, Y. Zhang, X. Shi and Q. Pan, *Surf. Coat. Technol.*, 2015, **272**, 221–228.
27 A. C. C. de Leon, R. B. Pernites and R. C. Advincula, *ACS Appl. Mater. Interfaces*, 2012, **4**, 3169–3176.
28 H. Bellanger, T. Darmanin, E. Taffin de Givenchy and F. Guittard, *Chem. Rev.*, 2014, **114**, 2694–2716.
29 Z. L. Wang, *ACS Nano*, 2008, **2**, 1987–1992.
30 H. Teisala, M. Tuominen, M. Aromaa, M. Stepien, J. M. Mäkelä, J. J. Saarinen, M. Toivakka and J. Kuusipalo, *Langmuir*, 2012, **28**, 3138–31458.
31 K. Liu, X. Yao and L. Jiang, *Chem. Soc. Rev.*, 2010, **39**, 3240–3255.
32 L. Gu, S. Liu, H. Zhao and H. Yu, *ACS Appl. Mater. Interfaces*, 2015, **7**, 17641–17648.
33 S. Liu, H. Sun, L. Sun and H. Fan, *Corros. Sci.*, 2012, **65**, 520–527.
34 Q. Liu, D. Chen and Z. Kang, *ACS Appl. Mater. Interfaces*, 2015, **7**, 1859–1867.
35 K. Zhang, J. Wu, P. Chu, Y. Ge, R. Zhao and X. Li, *Int. J. Electrochem. Sci.*, 2015, **10**, 6257–6272.
36 N. Wang, D. Xiong, Y. Deng, Y. Shi and K. Wang, *ACS Appl. Mater. Interfaces*, 2015, **7**, 6260–6272.
37 Q. Wang, X. Yao, H. Liu, D. Quéré and L. Jiang, *Proc. Natl. Acad. Sci. U. S. A.*, 2015, **112**, 9247–9252.
38 ASTM B117, Standard Practice for Operating Salt Spray (Fog) Apparatus, 2011.